Check for updates

Construction of a non-enzymatic electrochemical sensor based on graphitic carbon nitride nanosheets for sensitive detection of procalcitonin†

Yushuang Liu, [ID] * Furong Chen, Layue Bao and Wenfeng Hai [ID] *

In this study, we established a label free and ultrasensitive electrochemical sensor based on graphitic nitride nanosheets (g-C$_3$N$_4$ NS) for procalcitonin (PCT) detection. Firstly, an easy-to-prepare and well-conducting g-C$_3$N$_4$ NS was synthesized. Next the g-C$_3$N$_4$ NS was immobilized on the electrode surface by π–π stacking, and further used to anchor the specific recognition peptide (PP). The surface morphology and structure after g-C$_3$N$_4$ NS and PP modification was characterized by X-ray photoelectron spectroscopy (XPS), atomic force microscopy (AFM) and electrochemistry. The sensing property of this sensor was evaluated by differential pulse voltammetry (DPV) and showed a detection sensitivity with a dynamic range from 0.15 to 11.7 fg mL^{-1} with a low limit of detection (LOD) of 0.11 fg mL^{-1}. Besides, the electrochemical biosensor was successfully used to detect PCT in human serum samples, and the results suggest its potential use in clinical application.

1 Introduction

Sepsis is a critical whole-body inflammatory response due to microbial pathogen infection including by viruses, bacteria and fungi.[1,2] If sepsis is not treated carefully, it may cause a systemic inflammatory response, in severe cases leading to organ dysfunction and ultimately death.[3] Currently, sepsis is the main cause of death in Intensive Care Units (ICU) and its incidence is increasing worldwide with a mortality rate between 40 and 50% in developed countries and is responsible for more deaths than lung, breast and colon cancer combined.[2,4] Thus, there is an urgent need for rapid, reliable and simple methods for diagnosis of the origin of sepsis to enhance survival rate and patient outcomes.[5]

Currently, some biomarkers such as C-reactive protein (CRP), serum decoy receptor3 (DCR3), interleykin-6 (IL-6), tumor necrosis factor-α (TNF-α) and procalcitonin (PCT) have been investigated for the rapid identification of the origin of sepsis,[6,7] and these biomarkers have received the most attention in work focusing on sensor development. In comparison, PCT is generally accepted as the most promising biomarker because of its uniqueness and better sensitivity and selectivity.[8–10] In general, all of the PCT formed in C-cells and no PCT can enters

the circulation, so its level in healthy subjects is below the detection level. However, the PCT levels will be raised after the patients were infected with bacterial sepsis.[11,12] So far, there are diverse screening methods available for identifying the presence of infections including enzyme-linked immunosorbent assays (ELISA), blood cultures (BC),[13,14] molecular diagnostic techniques,[15] chemiluminescence immunoassay,[16] microfluidics immunoassays and fluorescence immunoassay. Due to the expensive and complicated instruments, tedious sample treatment, time-consuming in the detection system,[17,18] these methods can't meet the current needs for efficient and rapid detection of PCT. Hence, developing a sensitive and reliable method for PCT detection are required. Electrochemical methods with high sensitivity, selective, rapid response and portability have recently become burgeoning and powerful analytical methods.[19–21] The sensitivity of electrochemical sensor is mostly related to the choice of electrode materials. Thus, the researchers are focused on electrode modification and have studied a lot of materials for the electrochemical detection of biomaterials.[22]

Recently, graphitic carbon nitride (g-C$_3$N$_4$) with its graphite-like structure and commendable stability under ambient conditions, has received extensive attention due to its high stability, nontoxicity, facile and low-cost synthesis, appropriate band gap in the visible spectral.[23–25] In addition, as the most stable allotrope of carbon nitride semiconductor, it has become a promising material in photocatalysis, gas and fluorescent sensors, field emitter, electrode for fuel cells, and hydrogen storage for its abundant nitrogen active sites and unique

Inner Mongolia Key Laboratory of Carbon Nanomaterials, Nano Innovation Institute (NII), College Chemistry and Materials Science, Inner Mongolia University for Nationalities, Tongliao 028000, People's Republic of China. E-mail: yushuangliu1989@163.com

† Electronic supplementary information (ESI) available. See https://doi.org/10.1039/d2ra03650a

superior catalytic activity.[26,27] However, it is worth mentioning that as synthesized bulk g-C_3N_4 has poor conductivity, large band gap and low specific area, so it is not suitable for direct use in electrochemical sensing applications.

To conquer this problem, researchers have proposed various approaches (including the design of nanostructure, semiconductor composite, metal and non-metal mixtures) to enhance the electrochemical performance of g-C_3N_4.[28,29] Although modifying or doping methods have been proved effective on utilizing pure g-C_3N_4 for electrochemical sensing, new methods to change its own structural defects to enhance the electrochemical sensing are still necessary. Recently, g-C_3N_4 nanosheets (g-C_3N_4 NS) directly prepared by ultrasonication-assisted liquid exfoliation of bulk g-C_3N_4 provide an attractive option for bioprobes and bioimaging applications.[30] Like graphic or its derivatives, the graphite layer structure of g-C_3N_4 NS has higher specific surface area and provide more active sites. More importantly, some studies have shown that compared with the bulk g-C3N4, the g-C_3N_4 NS have better electrochemical activity and stability, suggesting that exfoliated ultrathin g-C_3N_4 NS are a promising candidate material for sensing application.[31–33]

Therefore, in this work, a novel and highly sensitive electrochemical sensor based on a g-C_3N_4 NS modified glass carbon electrode for the detection of PCT has been developed. The fabricated process of the sensor was presented in Scheme 1. Firstly, the g-C_3N_4 was synthesized and exfoliated by the ultrasonication and then directly drop-casting on the electrode surfaces (g-C_3N_4 NS/GCE), which could effectively promote the electrochemical signal due to the increase in surface area and deduction of the surface activation energy after the g-C_3N_4 NS modification. Subsequently, the probe peptide (PP) was linked onto the electrode surface via the π–π stacking between the g-C_3N_4 NS and phenylalanine at the end of the polypeptide, providing an effective electrochemical strategy for the sensitive determination of PCT. Otherwise, this sensor also exhibits excellent detection performance of PCT in real samples,

showing promising application in clinical test and disease diagnosis.

2 Experimental

2.1 Reagents and materials

Urea, sodium chloride (NaCl), potassium ferricyanide ($K_3Fe(CN)_6$) were obtained from Sinopharm Chemical Reagent Company (Shanghai, China). 1 M Tris–HCl, Bovine Serum Albumin (BSA) were supplied by Solarbio Company (Beijing, China). PCT, C-reaction protein and Interleukin-6 were purchased from Cusag Company (Wuhan, China). The capturing peptide powder was synthesized from Top-peptide Company (Shanghai, China), and the sequence of capturing peptide was displayed as follows:[34]

PP: TSCNGHTCTRPNF.

All experimental water was ultrapure water by Mill-Q water purification (18.2 MΩ).

2.2 Instrumentations

The morphology of electrode surface and the surface potential were observed by atomic force microscope (AFM, Asylum MFP-3D origin+, Oxford). The function groups and the structure of the g-C_3N_4 NS was characterized by Fourier Transform Infrared Spectrometer (FI-RT, Nicolet Impact 400D spectrometer) and X-ray diffraction spectrometer (XRD, Malvern Panalytical). All electrochemical measurements were performed using a multi-channel potentiostat (interface 1010, Gamry) via EC-lab software version. X-ray photoelectron spectroscopy (XPS) was conducted on an ESCALAB 250 spectrometer using AlKα radiation as the X-ray source (1486.7 eV) with the pass energy of 30 eV.

2.3 Preparation of ultrathin g-C_3N_4 nanosheets (NS)

The ultrathin g-C_3N_4 nanosheets (NS) were prepared with ultrasonication exfoliated method.[35,36] The detailed procedure is summarized as follows. The g-C_3N_4 bulk was produced by heating urea at 550 °C with a ramp rate of 5 °C min^{-1} and maintained at this temperature for another 3 h in argon environment, the yellow-colored power g-C_3N_4 was obtained.

To fabricate the g-C_3N_4 NS, 0.01 g bulk g-C_3N_4 power was added to 2 mL ethanol and ultrasonication for 1 h, afterward, the solution was allowed to stand undisturbed for overnight at room temperature to allow unexfoliated bulk g-C_3N_4 particles to settle at the bottom of the container.[37] The supernatant liquid (a homogenized dispersion) of exfoliated g-C_3N_4 NS was collected and used for further studies.

2.4 Fabrication of electrochemical biosensor

Prior to modification, the bare GCE was polished with 0.3 μm alumina slurry, then washed with water and ethanol repetitiously under ultrasonic treatment and dried with nitrogen gas. Next, 20 μL g-C_3N_4 NS suspension was dropped on the GCE surface (0.3 cm) and incubated for 3 h. After washed with Milli-Q water, 50 μL of 500 μM PP was dripped onto the surface of the modified electrode at 4 °C for 5 h, rinsed with Tris–HCl buffer.
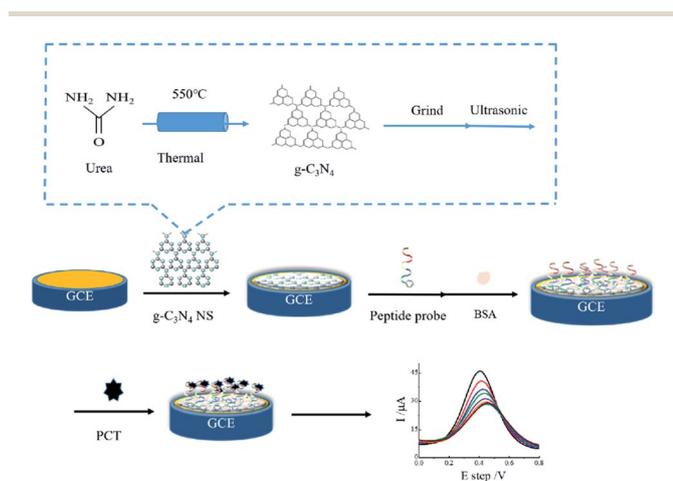
Scheme 1 Schematic representation for the fabrication of the PCT electrochemical biosensor.

The nonspecified binding sites were covered with 20 µL of BSA (2%, W/V).

2.5 General characterization

All electrochemical testing measurements were performed in a Tris–HCl solution containing 5 mM $K_3Fe(CN)_6/K_4Fe(CN)_6$. Three electrode consist of a bare or a modified GCE was used as working electrode, an Ag/AgCl (in 3.3 M KCl) as reference electrode and a Pt wire as counter electrode. The function groups of bulk $g-C_3N_4$ NS were characterized by FT-IR in the wavenumber range of 2400–400 cm^{-1}. The crystal structure of $g-C_3N_4$ NS were measured by using XRD in the 2θ range of 20° to 100° with CuKα radiation ($\lambda = 0.15406$). The surface morphologies of each fabrication steps were analysed by atomic force microscopy (AFM). All images were taken with a scan rate of 1 Hz at a scan range of 500 nm $\times$ 500 nm and XPS spectrometer which equipped with the AIKα radiation source and the takeoff angle of the photoelectron analyser was 90° respectively. The potential change of electrode surface was verified through AFM by the Scanning Kelvin Probe Microscopy (SKPM) mode.

2.6 PCT sensing

The PCT in range from 1 ag mL^{-1} to 10 ng mL^{-1} in Tris–HCl (pH 7.0) was measured by DPV (pulse time = 1) at room temperature. For the detection in serum sample, the human blood serum samples from healthy individuals were supplied by Affiliated Hospital of Inner Mongolia Minzu University under permission of the ethical committee of the university. And Informed consents were obtained from human participants of this study. The samples were centrifuged at 5000 rpm for 20 min, then filtered with 0.22 membrane, and the supernatant was used for the subsequent tests. In the recovery test, the collected serum was diluted 100 times using Tris–HCl buffer, and then PCT was added to obtain the final concentration. The recoveries were calculated from three concentrations of PCT spiked human serum samples. The mean and standard deviation were obtained from three independent tests.

3 Results and discussion

3.1 The morphology and structural information of the electrode surface

XPS was selected to identified the detail information of the $g-C_3N_4$ nanosheets. As shown in Fig. 1A, the peak for C, N, O can be seen. To locally enlarger view, the C1 peak can be deconvoluted to four peaks, which originate from the graphitic (284.3
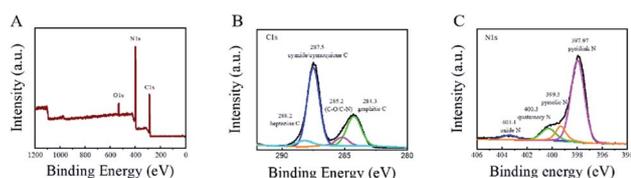

Fig. 1 XPS survey spectrum of $g-C_3N_4$ (A) and the related high-resolution spectra of C1s (B) and N1s(C) binding energy regions.

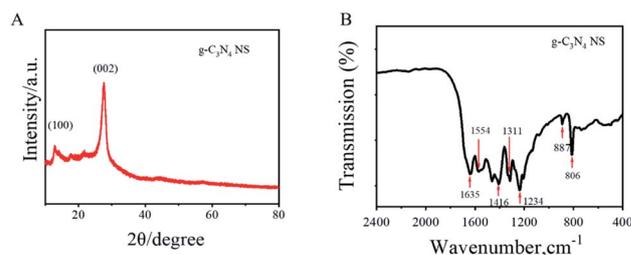**Fig. 2** (A) XRD pattern and (B) FT-IR spectrum of synthesized $g-C_3N_4$ NS.

eV), C–N/C–O bindings (285.2 eV), cyanide/cyanoquione (287.5 eV), and heptazine typed carbons (292.6 eV) respectively (Fig. 1B). For the N1s spectrum, the heptazine N (397.97 eV), pyrrolic N (399.3 eV), graphitic N (400.3 eV) and oxidic N (403.6 eV) can be deconvoluted respectively (Fig. 1C). All the characteristic peaks were in good agreement with the earlier reports of synthesized $g-C_3N_4$ NS.[35]

XRD patten and FT-IR spectrum were selected to determine the structure and the surface functional groups of the $g-C_3N_4$ nanosheets. For the XRD pattern, there were two distinct diffraction peaks can be found (Fig. 2A). The strongest peak at 27.62° is due to the stacking of the conjugated aromatic system, which is indexed for graphitic materials as the (002) peak and corresponding well to the interlayer d-spacing (0.336 nm) of the $g-C_3N_4$, indicating the formation of $g-C_3N_4$. The weak diffraction peak at 13.04° was assigned to the (100). The intensities of the diffraction peak at 13.04° become weaker with increasing heating temperatures, which indicate that the (100) crystal plane of $g-C_3N_4$ is slightly destroyed and the structure defects are formed when treated at high temperatures.[38]

Furthermore, for the FT-IR spectrum, the peaks at 1234 cm^{-1}, 1311 cm^{-1}, 1416 cm^{-1}, 1554 cm^{-1} and 1635 cm^{-1} correspond to the typical stretching vibration modes of C=N and C–N heterocycles.[39] The small peak located at 810 cm^{-1} is a signature of the characteristic breathing vibration mode of the triazine rings present in g-C3N4. The absorption feature at 889 cm^{-1} was associated to a deformation mode of cross-linked heptazine (Fig. 2B). All the characteristic peaks were good agreement with the prior reports on synthesized $g-C_3N_4$.

3.2 Characterization of the electrode

The morphological characterization of GCE surface was carried out by AFM. As shown in Fig. S1A,† the bare GCE surface was a relatively homogeneous flat structure, however, the electrode morphology changes significantly after the deposition of $g-C_3N_4$ NS and PP solution through the π–π stacking effect. The increased bright spots and the height indicate the successful modification of the electrode surface (Fig. S1B and C†).

XPS was used to obtain the detail information on the elemental and structural composition of the modified electrode surface. Based on the XPS survey scan results, the narrow scan spectrum of bare GCE shows a strong carbon (C1s) signal and tiny nitrogen (N1s) and sulfur (S2p) contribution (Fig. 3A–C). The N contribution increased significantly, and the S remains
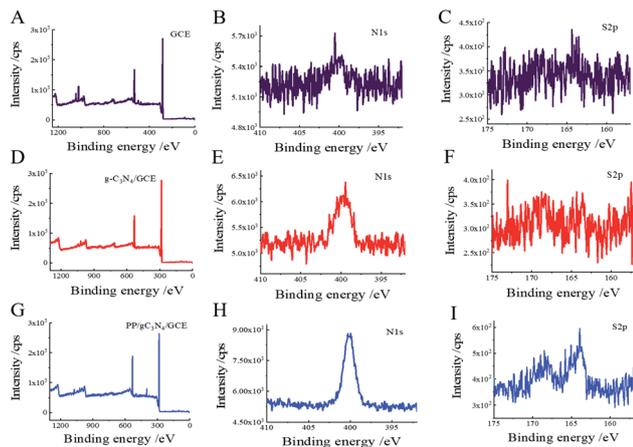
Fig. 3 XPS results following electrode modification. (A) Wide scan and narrow scan for (B) (N1s), and (C) (S2p) of the GCE. (D) Wide scan and narrow scan for (E) (N1s), and (F) (S2p) of the GCE surface after the g-C_3N_4 modified (g-C_3N_4/GCE). (G) Wide scan and narrow scan for (H) (N1s), and (I) (S2p) of the g-C_3N_4/GCE modified by peptide probe.

unchanged after the g-C_3N_4 NS modified (Fig. 3D–F). The results indicate that the g-C_3N_4 NS has been stacked on the electrode surface. After drop-casting the PP, the narrow scan spectrum shows clear peaks of S2p compared to the bare GCE and g-C_3N_4 NS/GCE (Fig. 3G–I), indicating the probe peptide can successfully anchor on the electrode surface through the π–π stacking forces. Otherwise, the changes in the content of N and S elements on the electrode surface also further prove the success of the electrode modifications (Table S1†).

The cyclic voltammetry (CV), differential pulse voltammetry (DPV) and electrochemical impedance spectroscopy (EIS) were used to demonstrate the stepwise modification of the electrode surface. In the terms of EIS, $[Fe(CN)_6]^{3-}/[Fe(CN)_6]^{4-}$ was utilized as the redox probe and the semicircle diameter was equal to electro-transfer resistance. In 5 mM $[Fe(CN)_6]^{3-/4-}$, bare

electrode exhibited almost a straight line (Fig. 4C), which was characteristic of a mass diffusion limiting step of the electro-transfer process. When the g-C_3N_4 NS and PP was self-assembled on to the electrode through the π–π stacking, the impedance increased, this can be attributed to g-C_3N_4 NS and PP can blocked the diffusion of the redox probe of $[Fe(CN)_6]^{3-/4-}$ and increased the interface electron transfer resistance.[40] The charge transfer resistance of each electrode was shown in Fig. 4D. These results were in good agreement with the obtained from CV and DPV measurements (Fig. 4A and B). Those results demonstrated that the sensing interface has been successfully fabricated.

3.3 Effect of scan rate

To study the controlled factor of the electrochemical process on the electrode surface, the impact of scan rates on the electrochemical behavior of 1 mM PCT at PP/g-C_3N_4 NS/GCE in 20 mM Tris–HCl was explored through the CV methods. As shown in Fig. 5A, the reduction peak currents of the sensor were observed to increase in linear correlation to the scan rate in the range of 10–100 mV s^{-1}. A linear dependency of the reduction peak currents on the scan rates was also obtained for the sensor in the presence of target PCT (Fig. 5B and C), which indicated that the electron transfer process of the modified electrode is diffusion-controlled.[41] The equation expressing the relationship can be written as follows:

$$I_{pa} \text{ (μA)} = 0.000004v^{1/2} + 7.5 \times 10^{-6}, R^2 = 0.99$$

$$\ln^{(I_{pa})} = 0.39 \ln^{(v)} - 2.12, R^2 = 0.99$$

3.4 Detection performance of the electrochemical biosensor

The performance of the PCT activity assay was carried out by exposing the substrate peptide probe on the biosensor to different concentrations of PCT under the same experimental conditions. Fig. 6A showed the DPV response of biosensor with different concentrations of PCT, the pulse time of DVP is 0.1 s (in Fig S2†). With increasing PCT concentration within the range of 0.15 fg mL^{-1} to 11.7 fg mL^{-1}, the electrochemical oxidation peak current decreased gradually, which attributed to the larger size PP-PCT complex hindered the diffusion of redox probe towards electrode surface and increased the electrode transfer resistance. Moreover, there was a linear relationship between DPV signal and ln(PCT) concentrations. The linear
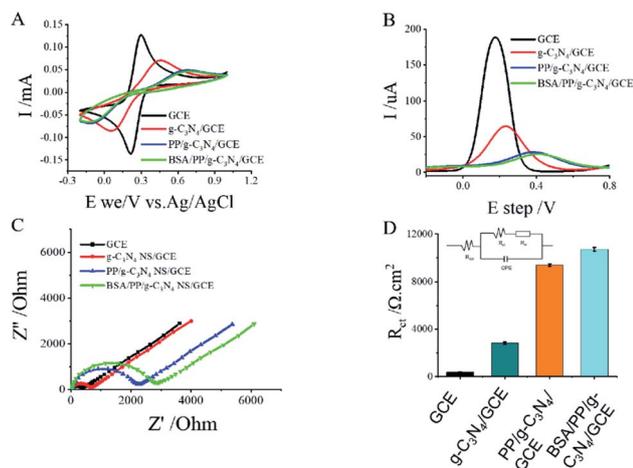
Fig. 4 (A) CVs of different electrodes. (B) DPV responses of different electrodes. (C) EIS response to different electrodes. (D) Charge transfer resistance (R_{ct}) for the different electrodes. Inset: corresponding equivalent circuit and modelling. The data are shown as the mean ± SD ($n = 3$).
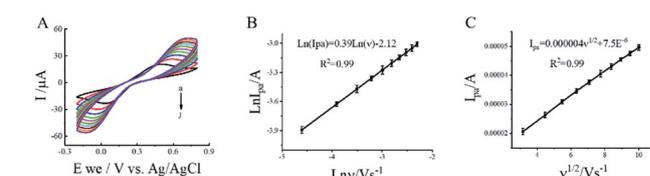
Fig. 5 (A) CVs of 1 mM PCT in 1 mL 20 mM Tris–HCl at various scan rates (10–100 mV). (B) and (C) are the calibration plot of the redox currents vs. scan rate. The data are shown as the mean ± SD ($n = 3$).
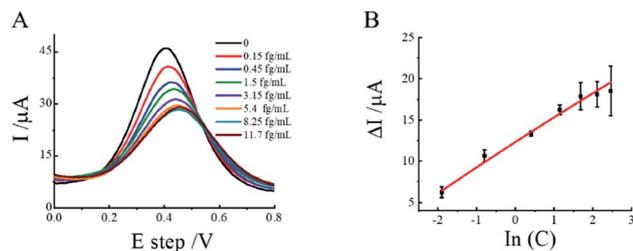
Fig. 6 Electrochemical detection of PCT using PP/g-C_3N_4 NS/GCE. (A) Changes in the DPV signals for the PP/g-C_3N_4 NS/GCE electrode at varying concentrations of PCT in 1 mL 20 mM Tris−HCl. (B) A plot of current change *versus* concentration of PCT. The data are shown as the mean ± SD ($n = 3$).

equation for PCT was described as $I(\mu A) = 3.02 \ln(C) + 12.88$ ($R^2 = 0.99$) and the detection limit were estimated to be 0.11 fg mL^{-1} (S/N = 3). Compared with other electrochemical methods, SPR biosensors and electrochemiluminescent immunosensor as list in Table S2,† our results present competitive detection limit. This result indicates that our devices can be used to detect the PCT and showed a better sensitivity compared with other reported methods.

For better understanding the mechanics of the higher detection sensitivity, SKPM measurements was performed. As shown in Fig. 7, the surface potential was increased about 0.3 V (from 0.9 V to 1.2 V) after the g-C_3N_4 NS was modified, which can promote the oxidation reaction due to the decrease in activation energy.[42]

In addition, we also calculated the electrode surface area after g-C_3N_4 NS modified. To calculated the electrochemically active surface areas, the CV of $K_3Fe(CN)_6/K_4Fe(CN)_6$ was analyzed by the Randles–Sevcik equation (eqn (1)):[43–45]

$$I_p = (2.69 \times 10^5)n^{3/2}AC^*D^{1/2}\nu^{1/2} \tag{1}$$

where I_p refers to the anodic peak current in amperes, n is the total number of electrons transferred ($n = 1$), A is the effective surface area of the electrons in cm^2, D is the diffusion coefficient for $K_3Fe(CN)_6/K_4Fe(CN)_6 = 7.6 \times 10^{-6}$ cm^2 s^{-1}, C^* is the concentration of $K_3Fe(CN)_6/K_4Fe(CN)_6$ in M cm^{-3} and ν is the scan rate in V s^{-1}. The effective surface areas of various electrodes were calculated from the slope of the I_p *versus* $\nu^{1/2}$ plot. The surface area of the GCE (0.07 cm^2) is less than the surface area of modified with g-C_3N_4 NS (0.09 cm^2). Which can expose more active sites and can bind more PP probes.[46,47] So, the larger
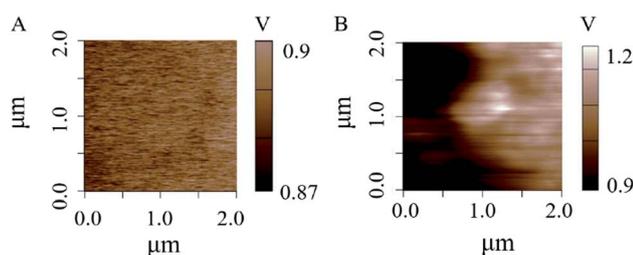

Fig. 7 SKPM image of the GCE surfaces. (A) Surface potential of GCE. (B) Surface potential of g-C_3N_4 NS/GCE.
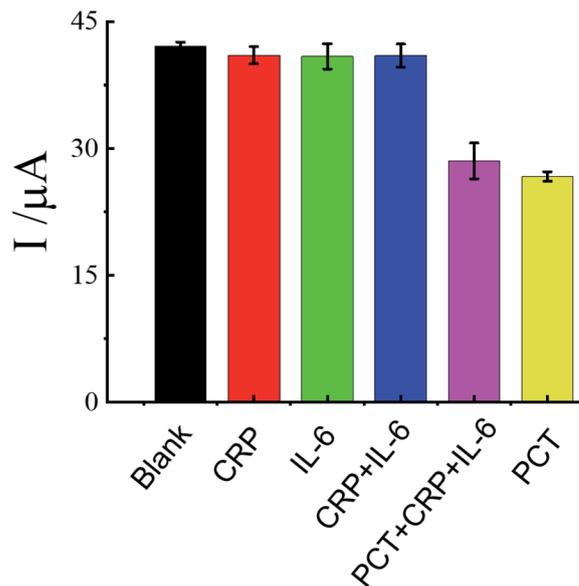

Fig. 8 The specificity and selectivity of the PP/g-C_3N_4 NS/GCE biosensor. The data are shown as the mean ± SD ($n = 3$).

surface area and the lower activation energy promote electrochemistry to display higher detection sensitivity.

3.5 Sensor specificity and real samples test

To evaluate the selectivity of the fabricated biosensor, several kinds of interference biomarkers were selected, including C-reaction protein (CRP), Interleukin-6 (IL-6). CRP is a biomarker of inflammation for the tissue damage and the IL-6 is related to multiple diseases such as diabetes osteoarthrosis, asthma and inflammatory bowel disease.[48] The concentration of PCT was 1 pg mL^{-1}, and the concentration of each interference biomarker was 10 fg mL^{-1}. Fig. 7 shows the DPV value for the samples spiked with each interference biomarker, PCT and the mixture with or without PCT individually. As shown in Fig. 8, the DPV value for each interference biomarker was very weak and similar to that of the control sample, however, the DPV value response of this sensor for the mixture of the PCT and each interference biomarker was same with that of PCT, this result demonstrate that the interference biomarker has no effect on the detection of the PCT, and inferred that the electrochemical sensor has highly specificity and selectivity.

To evaluate the practical application of PP/g-C_3N_4 NS electrochemical biosensors in blood sample, the concentration of PCT in human blood serum sample was analysed. Through the

Table 1 Determination of PCT in human serum samples

Samples	Added (fg mL^{-1})	Found (fg mL^{-1})	Recovery (%)	RSD[a] (%)
1	1	0.94	94	2.56
2	5	4.76	95.2	1.75
3	10	10.1	101	2.05

[a] RSD (%) was calculated from triple parallel experiments.

linear relationship established for the PP/g-C₃N₄/CGE PCT sensor, the recovery of the spiked PCT (1 fg mL⁻¹, 5 fg mL⁻¹, 10 fg mL⁻¹) range from 94 to 101.3% (in Table 1), indicating that the immune sensor based on PP/g-C₃N₄ NS/CGE had great potential for the analysis of PCT in real clinical samples.

4 Conclusions

A novel and sample electrochemical biosensor based on PP/g-C₃N₄ NS/GCE was developed and successfully used to detect the PCT. The larger surface area and lower active energy after g-C₃N₄ NS modified giving the electrochemical biosensor higher sensing capability. XPS, FT-IT, XRD were used to identified the structure and function groups of the g-C₃N₄ NS. AFM, CV, DPV and EIS measurements were used to identified the modification steps and the electrochemical performance. After that, a linear current response of PCT in the concentration range of 0.15 fg mL⁻¹ to 11.7 fg mL⁻¹ (R^2 = 0.99) and the LOD of 0.11 fg mL⁻¹ (S/N = 3) could be obtained. This sensitivity of our system was found to be comparable to that existing detection methods. Furthermore, PP/g-C₃N₄ NS/GCE produce good selectivity and better recovery in the real clinic samples. Those results indicated that the PCT biosensor designed by this work has the potential to solve the clinical rapid diagnosis and treatment of sepsis diseases worldwide.

Author contributions

Yushuag Liu: conceptualization, data curation, formal analysis, investigation, supervision writing. Furong Chen: resources. Layue Bao: resources. Wenfeng Hai: writing – Review.

Conflicts of interest

There are no conflicts to declare.

Acknowledgements

Notes and references

1 G. Sener, E. Ozgur, A. Y. Rad, L. Uzun, R. Say and A. Denizli, Rapid real-time detection of procalcitonin using a microcontact imprinted surface plasmon resonance biosensor, *Analyst*, 2013, **138**(21), 6422–6428.

2 N. Fabri-Faja, O. Calvo-Lozano, P. Dey, R. A. Terborg, M. C. Estevez, A. Belushkin, F. Yesilköy, L. Duempelmann, H. Altug, V. Pruneri and L. M. Lechuga, Early sepsis diagnosis via protein and miRNA biomarkers using a novel point-of-care photonic biosensor, *Anal. Chim. Acta*, 2019, **1077**, 232–242.

3 K. Essandoh and G.-C. Fan, Role of extracellular and intracellular microRNAs in sepsis, *Biochim. Biophys. Acta, Mol. Basis Dis.*, 2014, **1842**(11), 2155–2162.

4 C. Russell, A. C. Ward, V. Vezza, P. Hoskisson, D. Alcorn, D. P. Steenson and D. K. Corrigan, Development of a needle shaped microelectrode for electrochemical detection of the sepsis biomarker interleukin-6 (IL-6) in real time, *Biosens. Bioelectron.*, 2019, **126**, 806–814.

5 B. Pejcic, R. De Marco and G. Parkinson, The role of biosensors in the detection of emerging infectious diseases, *Analyst*, 2006, **131**(10), 1079–1090.

6 T. J. Durkin, B. Barua and S. Savagatrup, Rapid Detection of Sepsis: Recent Advances in Biomarker Sensing Platforms, *ACS Omega*, 2021, **6**(47), 31390–31395.

7 C. Pierrakos, D. Velissaris, M. Bisdorff, J. C. Marshall and J.-L. Vincent, Biomarkers of sepsis: time for a reappraisal, *Crit. Care*, 2020, **24**(1), 287.

8 H. El Haddad, A.-M. Chaftari, R. Hachem, P. Chaftari and I. I. Raad, Biomarkers of Sepsis and Bloodstream Infections: The Role of Procalcitonin and Proadrenomedullin With Emphasis in Patients With Cancer, *Clin. Infect. Dis.*, 2018, **67**(6), 971–977.

9 H. Medetalibeyoglu, M. Beytur, O. Akyıldırım, N. Atar and M. L. Yola, Validated electrochemical immunosensor for ultra-sensitive procalcitonin detection: carbon electrode modified with gold nanoparticles functionalized sulfur doped MXene as sensor platform and carboxylated graphitic carbon nitride as signal amplification, *Sens. Actuators, B*, 2020, **319**, 128195.

10 C. Pierrakos and J.-L. Vincent, Sepsis biomarkers: a review, *Crit. Care*, 2010, **14**(1), 1–18.

11 N. G. Morgenthaler, J. Struck, Y. Chancerelle, W. Weglöhner, D. Agay, C. Bohuon, V. Suarez-Domenech, A. Bergmann and B. Müller, Production of procalcitonin (PCT) in non-thyroidal tissue after LPS injection, *Horm. Metab. Res.*, 2003, **35**(5), 290–295.

12 W.-J. Shen, Y. Zhuo, Y.-Q. Chai, Z.-H. Yang, J. Han and R. Yuan, Enzyme-Free Electrochemical Immunosensor Based on Host–Guest Nanonets Catalyzing Amplification for Procalcitonin Detection, *ACS Appl. Mater. Interfaces*, 2015, **7**(7), 4127–4134.

13 N. Mancini, R. Burioni, M. Clementi, Microbiological Diagnosis of Sepsis: the Confounding Effects of a "Gold Standard", in *Sepsis: Diagnostic Methods and Protocols*, ed. N. Mancini, Springer New York, New York, NY, 2015, pp. 1–4.

14 J. AlvArez, J. Mar, E. Varela-Ledo, M. Garea, L. Matinez-lamas, J. Rodriguez and B. Regueiro, Cost analysis of real-time polymerase chain reaction microbiological diagnosis in patients with septic shock, *Anaesth. Intensive Care*, 2012, **40**, 958–963.

15 A. M. Caliendo, D. N. Gilbert, C. C. Ginocchio, K. E. Hanson, L. May, T. C. Quinn, F. C. Tenover, D. Alland, A. J. Blaschke, R. A. Bonomo, K. C. Carroll, M. J. Ferraro, L. R. Hirschhorn, W. P. Joseph, T. Karchmer, A. T. MacIntyre, L. B. Reller, A. F. Jackson and America f. t. I. D. S. o., Better Tests,

Better Care: Improved Diagnostics for Infectious Diseases, *Clin. Infect. Dis.*, 2013, **57**(suppl. 3), S139–S170.

16 N. G. Morgenthaler, J. Struck, C. Fischer-Schulz and A. Bergmann, Sensitive immunoluminometric assay for the detection of procalcitonin, *Clin. Chem.*, 2002, **48**(5), 788–790.

17 G. Li, Y. Wu, Y. Li, Y. Hong, X. Zhao, P. I. Reyes and Y. Lu, Early stage detection of Staphylococcus epidermidis biofilm formation using MgZnO dual-gate TFT biosensor, *Biosens. Bioelectron.*, 2020, **151**, 111993.

18 H. Yin, M. Wang, B. Li, Z. Yang, Y. Zhou and S. Ai, A sensitive electrochemical biosensor for detection of protein kinase A activity and inhibitors based on Phos-tag and enzymatic signal amplification, *Biosens. Bioelectron.*, 2015, **63**, 26–32.

19 M. La, Electrochemical, Electrochemiluminescent and Photoelectrochemical Immunosensors for Procalcitonin Detection: A Review, *Int. J. Electrochem. Sci.*, 2020, **15**, 6436–6447.

20 A. R. Correia, I. Sampaio, E. J. Comparetti, N. C. S. Vieira and V. Zucolotto, Optimized PAH/Folic acid layer-by-layer films as an electrochemical biosensor for the detection of folate receptors, *Bioelectrochemistry*, 2021, **137**, 107685.

21 Y. Liu, H. Li, S. Gong, Y. Chen, R. Xie, Q. Wu, J. Tao, F. Meng and Z. Peng, A novel non-enzymatic electrochemical biosensor based on the nanohybrid of bimetallic PdCu nanoparticles/carbon black for highly sensitive detection of H_2O_2 released from living cells, *Sens. Actuators, B*, 2019, **290**, 249–257.

22 K. Atacan and M. Özacar, Construction of a non-enzymatic electrochemical sensor based on CuO/g-C3N4 composite for selective detection of hydrogen peroxide, *Mater. Chem. Phys.*, 2021, **266**, 124527.

23 K. Dhara and D. R. Mahapatra, Recent advances in electrochemical nonenzymatic hydrogen peroxide sensors based on nanomaterials: a review, *J. Mater. Sci.*, 2019, **54**(19), 12319–12357.

24 G. Liao, F. He, Q. Li, L. Zhong, R. Zhao, H. Che, H. Gao and B. Fang, Emerging graphitic carbon nitride-based materials for biomedical applications, *Prog. Mater. Sci.*, 2020, **112**, 100666.

25 J. Zhu, W. Nie, Q. Wang, J. Li, H. Li, W. Wen, T. Bao, H. Xiong, X. Zhang and S. Wang, In situ growth of copper oxide-graphite carbon nitride nanocomposites with peroxidase-mimicking activity for electrocatalytic and colorimetric detection of hydrogen peroxide, *Carbon*, 2018, **129**, 29–37.

26 X. Li, J. Zhang, L. Shen, Y. Ma, W. Lei, Q. Cui and G. Zou, Preparation and characterization of graphitic carbon nitride through pyrolysis of melamine, *Appl. Phys. A*, 2009, **94**(2), 387–392.

27 T. Jiang, G. Jiang, Q. Huang and H. Zhou, High-sensitive detection of dopamine using graphitic carbon nitride by electrochemical method, *Mater. Res. Bull.*, 2016, **74**, 271–277.

28 Y. Cao, L. Wang, C. Wang, X. Hu, Y. Liu and G. Wang, Sensitive detection of glyphosate based on a Cu-BTC MOF/ g-C3N4 nanosheet photoelectrochemical sensor, *Electrochim. Acta*, 2019, **317**, 341–347.

29 L. F. Gao, T. Wen, J. Y. Xu, X. P. Zhai, M. Zhao, G. W. Hu, P. Chen, Q. Wang and H. L. Zhang, Iron-Doped Carbon Nitride-Type Polymers as Homogeneous Organocatalysts for Visible Light-Driven Hydrogen Evolution, *ACS Appl. Mater. Interfaces*, 2016, **8**(1), 617–624.

30 J. Tian, Q. Liu, C. Ge, Z. Xing, A. M. Asiri, A. O. Al-Youbi and X. Sun, Ultrathin graphitic carbon nitride nanosheets: a low-cost, green, and highly efficient electrocatalyst toward the reduction of hydrogen peroxide and its glucose biosensing application, *Nanoscale*, 2013, **5**(19), 8921–8924.

31 X. Zhang, X. Xie, H. Wang, J. Zhang, B. Pan and Y. Xie, Enhanced Photoresponsive Ultrathin Graphitic-Phase C3N4 Nanosheets for Bioimaging, *J. Am. Chem. Soc.*, 2013, **135**(1), 18–21.

32 P. Niu, L. Zhang, G. Liu and H. M. Cheng, Graphene-like carbon nitride nanosheets for improved photocatalytic activities, *Adv. Funct. Mater.*, 2012, **22**(22), 4763–4770.

33 J. Tian, Q. Liu, A. M. Asiri, A. H. Qusti, A. O. Al-Youbi and X. Sun, Ultrathin graphitic carbon nitride nanosheets: a novel peroxidase mimetic, Fe doping-mediated catalytic performance enhancement and application to rapid, highly sensitive optical detection of glucose, *Nanoscale*, 2013, **5**(23), 11604–11609.

34 J. M. Lim, M. Y. Ryu, J. H. Kim, C. H. Cho, T. J. Park and J. P. Park, An electrochemical biosensor for detection of the sepsis-related biomarker procalcitonin, *RSC Adv.*, 2017, **7**(58), 36562–36565.

35 J. Liu, S. Xie, Z. Geng, K. Huang, L. Fan, W. Zhou, L. Qiu, D. Gao, L. Ji, L. Duan, L. Lu, W. Li, S. Bai, Z. Liu, W. Chen, S. Feng and Y. Zhang, Carbon Nitride Supramolecular Hybrid Material Enabled High-Efficiency Photocatalytic Water Treatments, *Nano Lett.*, 2016, **16**(10), 6568–6575.

36 F. Yang, X. Wang, Q. Hu, D. Jiang, Y. Lu, Y. Wang, J. Wang and J. Liu, Carbon nitride initiated photopolymerization into a luminescent elastomer hydrogel, *Mater. Chem. Front.*, 2021, **5**(17), 6491–6501.

37 N. Murugan, M. B. Chan-Park and A. K. Sundramoorthy, Electrochemical Detection of Uric Acid on Exfoliated Nanosheets of Graphitic-Like Carbon Nitride (g-C_3N_4) Based Sensor, *J. Electrochem. Soc.*, 2019, **166**(9), B3163–B3170.

38 L. Ge, Synthesis and photocatalytic performance of novel metal-free g-C3N4 photocatalysts, *Mater. Lett.*, 2011, **65**(17), 2652–2654.

39 T. Di, B. Zhu, B. Cheng and J. Yu, A direct Z-scheme g-C_3N_4/ SnS_2 photocatalyst with superior visible-light CO_2 reduction performance, *J. Catal.*, 2017, **352**, 532–541.

40 A. S. Tanak, B. Jagannath, Y. Tamrakar, S. Muthukumar and S. J. A. c. a. X. Prasad, Non-faradaic electrochemical impedimetric profiling of procalcitonin and C-reactive protein as a dual marker biosensor for early sepsis detection, *Anal. Chim. Acta: X*, 2019, **3**, 100029.

41 X. Tian, C. Cheng, H. Yuan, J. Du, D. Xiao, S. Xie and M. M. Choi, Simultaneous determination of L-ascorbic acid, dopamine and uric acid with gold nanoparticles-β-cyclodextrin-graphene-modified electrode by square wave voltammetry, *Talanta*, 2012, **93**, 79–85.

42 J. O. M. Bockris and A. K. Reddy, Ion—Solvent Interactions, in *Modern electrochemistry*, Springer, 1970, pp. 45–174.

43 K. J. J. o. A. Atacan, Compounds, CuFe2O4/reduced graphene oxide nanocomposite decorated with gold nanoparticles as a new electrochemical sensor material for L-cysteine detection, *J. Alloys Compd.*, 2019, **791**, 391–401.

44 N. Demir, K. Atacan, M. Ozmen and S. Z. Bas, Design of a new electrochemical sensing system based on MoS2–TiO2/reduced graphene oxide nanocomposite for the detection of paracetamol, *New J. Chem.*, 2020, **44**(27), 11759–11767.

45 A. Jirjees Dhulkefl, K. Atacan, S. Z. Bas and M. Ozmen, An Ag–TiO2–reduced graphene oxide hybrid film for electrochemical detection of 8-hydroxy-2′-deoxyguanosine

as an oxidative DNA damage biomarker, *Anal. Methods*, 2020, **12**(4), 499–506.

46 T. Kamata, D. Kato and O. Niwa, Electrochemical performance at sputter-deposited nanocarbon film with different surface nitrogen-containing groups, *Nanoscale*, 2019, **11**(21), 10239–10246.

47 Y. Li, J. Zhou, J. Song, X. Liang, Z. Zhang, D. Men, D. Wang and X.-E. Zhang, Chemical nature of electrochemical activation of carbon electrodes, *Biosens. Bioelectron.*, 2019, **144**, 111534.

48 J. Wu, Y. Xianyu, X. Wang, D. Hu, Z. Zhao, N. Lu, M. Xie, H. Lei and Y. Chen, Enzyme-Free Amplification Strategy for Biosensing Using Fe3+–Poly(glutamic acid) Coordination Chemistry, *Anal. Chem.*, 2018, **90**(7), 4725–4732.